

Global Forebrain Dynamics Predict Rat Behavioral States and Their Transitions

Damien Gervasoni,^{1*} Shih-Chieh Lin,^{1*} Sidarta Ribeiro,^{1*} Ernesto S. Soares,¹ Janaina Pantoja,¹ and Miguel A. L. Nicolelis^{1,2,3,4}

Departments of ¹Neurobiology, ²Biomedical Engineering, and ³Psychological Brain Sciences and ⁴Center for Neuroengineering, Duke University Medical Center, Durham, North Carolina 27710

The wake–sleep cycle, a spontaneous succession of global brain states that correspond to major overt behaviors, occurs in all higher vertebrates. The transitions between these states, at once rapid and drastic, remain poorly understood. Here, intracranial local field potentials (LFPs) recorded in the cortex, hippocampus, striatum, and thalamus were used to characterize the neurophysiological correlates of the rat wake–sleep cycle. By way of a new method for the objective classification and quantitative investigation of all major brain states, we demonstrate that global brain state transitions occur simultaneously across multiple forebrain areas as specific spectral trajectories with characteristic path, duration, and coherence bandwidth. During state transitions, striking changes in neural synchronization are effected by the prominent narrow-band LFP oscillations that mark state boundaries. Our results demonstrate that distant forebrain areas tightly coordinate the processing of neural information during and between global brain states, indicating a very high degree of functional integration across the entire wake–sleep cycle. We propose that transient oscillatory synchronization of synaptic inputs, which underlie the rapid switching of global brain states, may facilitate the exchange of information within and across brain areas at the boundaries of very distinct neural processing regimens.

Key words: local field potentials; behavior; coherence; synchronization; sleep; state mapping

Introduction

Cortical electrical activity reflects the different behavioral states that comprise the wake–sleep cycle in higher vertebrates (Caton, 1875; Berger, 1929; Dement and Kleitman, 1957; Timo-Iaria et al., 1970). During waking, cortical regions produce low-amplitude fast oscillations (beta and gamma frequency bands, >15 Hz) (Steriade et al., 1993; Destexhe et al., 1999). In contrast, the onset of sleep is marked by high-amplitude, slow cortical oscillations in different frequency bands (delta waves at 1–4 Hz and spindles at 7–14 Hz) (Steriade et al., 1993; Achermann and Borbély, 1997; Werth et al., 1997; Destexhe et al., 1999), characterizing a behavioral state called slow-wave sleep (SWS). This state is followed by the highly oscillatory and transient intermediate sleep stage (IS) (Gottesmann, 1973, 1996; Mandile et al., 1996). During the ensuing rapid eye movement (REM) sleep (Dement and Kleitman, 1957; Jouvet, 1962; Moruzzi, 1972) the

cortex is ridden by low-amplitude, fast oscillations similar to those of alert waking (Vanderwolf, 1969; Steriade et al., 1993). In rodents, REM sleep is also characterized by highly conspicuous theta oscillations (5–9 Hz) in the hippocampus (Vanderwolf, 1969), nearly identical to the alert waking pattern (Winson, 1974). An additional transient waking state characterized by synchronized whisker twitching (WT) and cortico-thalamic local field potential (LFP) oscillations at 7–12 Hz occurs in rats (Nicolelis et al., 1995; Fanselow and Nicolelis, 1999), resembling mu rhythm in humans (Gastaut, 1952; Hari and Salmelin, 1997). These prominent oscillations have been demonstrated recently to define a physiological state associated with normal sensory perception (Fanselow and Nicolelis, 1999; Nicolelis and Fanselow, 2002; Wiest and Nicolelis, 2003).

Despite the ubiquity of behavioral states alternation, its dynamics remain poorly understood. Functional imaging has provided recent advances but with limited temporal resolution (Maquet, 1997, 1999; Hobson and Pace-Schott, 2002). At present, an objective and comprehensive account of the rapid switching between global brain states is still missing. To address this issue, we characterized in rats the dynamics of large-scale forebrain neural ensembles throughout the wake–sleep cycle, with a focus on spontaneous state transitions. The relationship between different behavioral states and concurrent intracranial LFPs recorded in multiple forebrain areas was analyzed with a novel multidimensional state-mapping technique based on two spectral ratios and a coherence measure. Our state maps, solely based on the collectively recorded electrical activity of forebrain neural ensembles,

Received April 22, 2004; revised Oct. 20, 2004; accepted Oct. 25, 2004.

This work was supported by National Institutes of Health Grants 5 R01 DE11451 and R01 DE13810, Defense Advanced Research Projects Agency Grant N66001-01-C-8062 (M.A.L.N.), an Institut National de la Santé et de la Recherche Médicale fellowship (D.G.), and a fellowship from the Pew Latin American Fellows Program in the Biomedical Sciences (S.R.). We thank G. Lehw and J. Meloy for manufacturing multielectrode arrays and for outstanding electronic support; C. Henriquez and J. Pormann for computer cluster administration; H. Wiggins for continuous technical support; L. Oliveira, G. Wood, and L. Hawkey for miscellaneous support; and S. Halkiotis for proofreading of this manuscript.

*D.G., S.-C.L., and S.R. contributed equally to this work.

Correspondence should be addressed to Damien Gervasoni, Department of Neurobiology, Duke University Medical Center, Research Drive, Box 3209, Durham, NC 27710. E-mail: gervasoni@neuro.duke.edu.

DOI:10.1523/JNEUROSCI.3524-04.2004

Copyright © 2004 Society for Neuroscience 0270-6474/04/2411137-11\$15.00/0

precisely predict the occurrence of the five major behavioral states that comprise the rat wake–sleep cycle, as well as some of their respective substates. Most importantly, our new method allowed for a quantitative and systematic investigation of global state transitions. We found that these transitions invariably occur simultaneously in distinct forebrain structures as fast changes in the oscillatory synchronization of synaptic inputs.

Materials and Methods

Surgical procedures and recordings. Five adult male Long–Evans rats (250–300 gm) were chronically implanted with tungsten microwire (diameter of 35 μm , impedance $\geq 1\text{ M}\Omega$ measured at 1 kHz) multielectrode arrays placed into four brain areas for simultaneous recordings: the primary somatosensory “barrel” cortex (Cx), the ventral posterior medial nucleus of the thalamus (Th), the dorsal caudate–putamen (CP), and the hippocampus (Hi). These areas of interest were chosen so as to comprise three forebrain circuits related to vital functions for rats: the thalamo-cortical loop plays a key role in sensory coding (Steriade, 1993; Nicolelis et al., 1995; Singer, 1995; McCormick and Bal, 1997; Engel et al., 2001) and is critically involved in the generation of state-related rhythms (McCormick, 2002; Steriade, 2003); the hippocampo-cortical loop is involved in spatial information processing and memory formation (Bland, 1986; McNaughton et al., 1986; Squire, 1986; Buzsaki et al., 1990; Wilson and McNaughton, 1994), and the cortico-striatal loop is involved in the execution of complex motor sequences (Graybiel, 1997), as well as sensory and cognitive functions (Brown et al., 1997; Blazquez et al., 2002). Implants were guided by standard stereotaxic coordinates (Paxinos and Watson, 1998) and concurrent physiological recordings, as described previously (Nicolelis et al., 1997, 2003). The following coordinates relative to bregma were used to center the arrays (in mm): Cx, +3.0 antero-posterior (AP), +5.5 mediolateral (ML), –1.5 dorsoventral (DV); Th, +3.0 AP, +3.0 ML, –5.0 DV; CP, –1.0 AP, +2.8 ML, –4.0 DV; and Hi, +2.8 AP, +1.5 ML, –3.3 DV. Hippocampal data pool together signals recorded with staggered electrodes from the CA1 field and the dentate gyrus. The locations of implants were histologically verified by comparing cresyl-stained frontal brain sections with reference anatomical planes (Paxinos and Watson, 1998). All electrode arrays were found at the expected position. After a postoperative recovery period (15 d), animals were individually habituated to a recording chamber (39 \times 32 cm) for 5 d under a 12 hr light/dark cycle (lights on at 6:00 A.M.; water and food *ad libitum*). Animals were continuously recorded for 48, 96, or 120 hr ($n = 2, 2, \text{ and } 1$, respectively). LFPs were preamplified (500 \times), filtered (0.3–400 Hz), and digitized at 500 Hz using a Digital Acquisition card (National Instruments, Austin, TX) and a Multi-Neuron Acquisition Processor (Plexon, Dallas, TX). Behaviors were recorded by way of two CCD video cameras and a video cassette recorder; infrared illumination was used during the dark phase of the night. Video and neural recordings were synchronized with a millisecond-precision timer (model VTG-55; For-A, Tokyo, Japan). Animal care was performed in accordance with the National Institutes of Health guidelines and the Duke University Institutional Animal Care and Use Committee.

Behavioral analysis. Two well trained experimenters visually coded the behavioral states by inspection of behaviors and associated LFP spectral features (see Fig. 1*A, B*). Five behavioral states were coded (Timon-Laria et al., 1970; Winson, 1974; Fanselow and Nicolelis, 1999). (1) In active exploration (AE), the animal engaged in exploratory behavior (locomotion, whisking, and sniffing), with low-amplitude cortical LFPs and high theta (5–9 Hz) and gamma (30–55 Hz) power density. (2) In quiet waking (QW), the animal was immobile (standing or sitting quietly) or engaged in “automatic” stereotyped behaviors (eating, drinking, and grooming), with low-amplitude cortical LFPs and relatively high theta and gamma activity but less than during AE. (3) In WT, the animal was immobile and standing, with rhythmic whisker movements (twitching) at the same frequency of underlying cortical-thalamic oscillations (7–12 Hz) (Fanselow and Nicolelis, 1999). (4) In SWS, the animal was lying immobile with eyes closed and slow regular respiratory movements. It begins with sleep spindles (10–14 Hz) superimposed to delta waves (1–4 Hz). As SWS deepens, delta oscillations become predominant, although

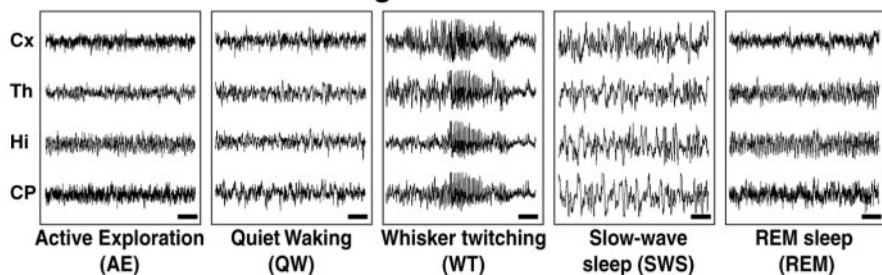
isolated spindles can still be observed. (5) In REM, the animal was immobile and atonic except for intermittent whisker and ear twitches, with low cortical LFP amplitude and very high theta and gamma power. Epochs containing spindles associated with hippocampal theta rhythm (intermediate sleep) were at that point scored as part of REM episodes (Gottesmann, 1973; Mandile et al., 1996). The amount of time spent in each behavioral state and the probability of transition between states were quantified (see supplemental Fig. S1, available at www.jneurosci.org as supplemental material). In agreement with previous studies, we found that rats spent $\sim 60\%$ of the day (lights on) sleeping and $\sim 60\%$ of the night (lights off) awake. We also corroborated the observation (Piscopo et al., 2001) that some state transitions are highly prevalent (e.g., AE \leftrightarrow QW, QW \leftrightarrow SWS, QW \leftrightarrow WT, SWS \rightarrow REM, and REM \rightarrow QW), whereas others are either very rare (SWS \rightarrow AE, REM \rightarrow AE, and WT \rightarrow AE) or absent (SWS \rightarrow WT and AE \rightarrow REM).

Construction of the two-dimensional state space. To gain insight into the dynamics of spontaneous brain states and their transitions, a two-dimensional (2-D) state space was defined by two spectral amplitude ratios calculated by dividing integrated spectral amplitudes at selected frequency bands from LFPs simultaneously recorded in the four areas of interest. First, all data segments with amplitude saturation were discarded from the working dataset (0.41–0.79% of the total data per rat). With Matlab (MathWorks, Natick, MA), a sliding window Fourier transform was applied to each LFP signal using a 2 sec window with a 1 sec step (see Fig. 1*C*). The Fourier transform parameters were chosen to allow for a frequency resolution of 0.5 Hz. Then, two spectral amplitude ratios were calculated by integrating the spectral amplitude (absolute value) over selected frequency bands for each data window: 0.5–20/0.5–55 Hz for ratio 1 and 0.5–4.5/0.5–9 Hz for ratio 2. These ratios are heuristic, resulting from a thorough search for parameters aimed at the best separation of states. The ratio measures were designed to produce normalized values bounded between 0 and 1, i.e., the frequency range of the numerator was always included in the denominator to yield more symmetrical distributions. A low-cut frequency of 0.5 Hz was used to eliminate the DC component. For each animal, principal component analysis (PCA) was applied to the same spectral amplitude ratio obtained from all LFP channels, and the first principal component (PC) was used as the overall ratio measure, typically explaining 80% of the variance. Resulting PCs were further smoothed with a Hanning window of 20 sec to reduce within-state variability. These two ratios were used to construct the 2-D state space in which each point represents 1 sec of ongoing brain activity. The density of points therefore reflects the relative abundance of the different brain states, and the distance between two consecutive data points reflects the speed of spectral changes.

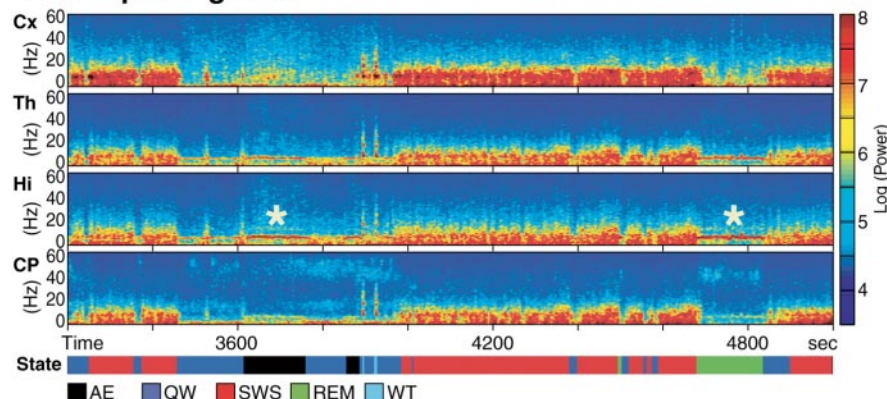
Trajectory analysis. Consecutive points in the 2-D state space can be linked to form spectral trajectories, representing state evolution over time. Trajectories connecting distinct clusters thus represent transitions between states. Cluster boundaries were algorithmically delineated as follows. For each animal, enhanced maps were generated by dividing the point density of 2-D maps (density plot) by the square of the average spectral change speed at each bin (speed plot). One hundred linearly spaced contours covering the whole range of the enhanced map were calculated, and sets of mutually excluding concentric contours corresponding to the main clusters were identified. Within each cluster-specific set of contours, the 95% most-inclusive contour was chosen as the initial boundary of each cluster, resulting in non-overlapping state-specific limits (see supplemental Fig. S5, available at www.jneurosci.org as supplemental material). Trajectories connecting different clusters were considered to be valid transitions if (1) the duration of the trajectory connecting two different clusters was < 60 sec and (2) the trajectory spent at least half of the preceding 30 sec in the initiating cluster and half of the 30 subsequent sec in the terminating cluster.

Coherence analysis. Coherence is the conventional technique to determine the spectral coupling among signals from different brain regions (Achermann and Borbely, 1998a), and can be used to address the large-scale functional connectivity between brain regions (Achermann and Borbely, 1998a; Nunez, 2000): high coherence in a particular range of frequencies reveals simultaneous and phase-locked oscillatory activity in the brain structures from which the records are derived. To calculate

A Intracranial LFP recordings



B LFP Spectrograms



C Construction of the 2D state-space

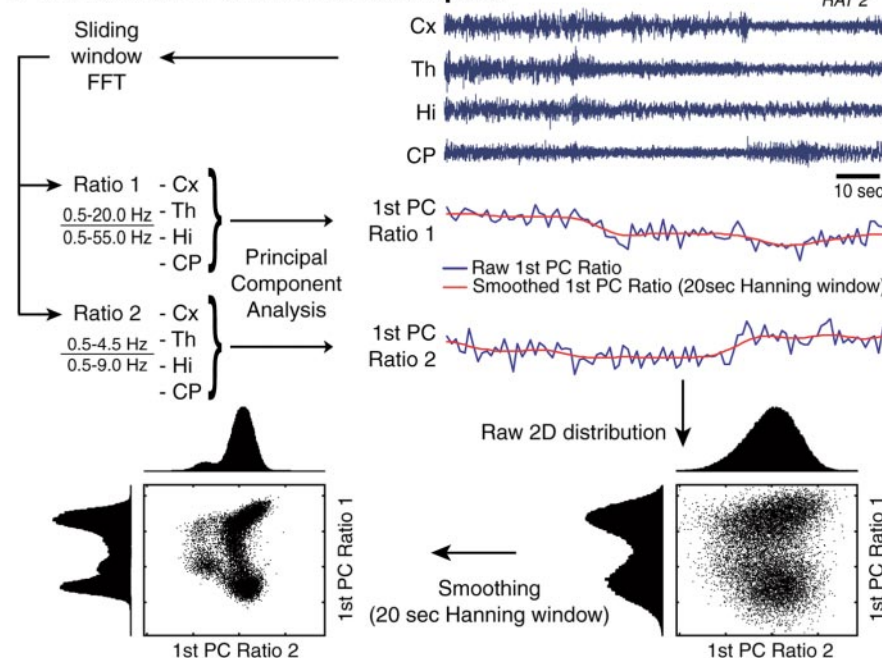


Figure 1. Intracranial local field potentials and behavioral states. *A*, Raw simultaneous LFP recordings in the four areas of interest. Calibration bar, 1 sec. Five brain states were initially distinguished by visual inspection of LFP traces and behavior. *B*, LFP power spectrograms, aligned with the color-coded hypnogram, i.e., the temporal sequence of the behavioral states assessed by visual observation of the behavior and inspection of the concurrent LFP features. All areas show simultaneous state-dependent variations of LFP spectral pattern. Notice that AE (black) and REM (green) both show pronounced theta rhythm (white asterisk). *C*, Construction of the 2-D state space. After elimination of segments with amplitude saturation (representing <1% of the total duration in each rat), a sliding window Fourier transform was applied to each LFP signal to calculate two spectral amplitude ratios. PCA was then applied to these ratios obtained from all LFP channels, and the first PC was used as the overall ratio measure. These measures obtained for each second of data were further smoothed with a Hanning window (20 sec length). Plotted against each other, the two first PCs of spectral ratios define the 2-D state space. Note that clear cluster structures emerged in the 2-D state space after smoothing (the 1-D histogram became more compact after smoothing).

coherence, a moving-window analysis was performed on 8 sec LFP segments, each multiplied by a Hanning window of equal length. Each segment was then broken down into multiple 1 sec segments (with 0.5 sec overlapping) in which coherence was calculated. This constitutes a sliding snapshot of coherence assigned to the middle timestamp of the 8 sec segment, i.e., coherence at time t sec was actually calculated in the interval $[t - 4, t + 4]$ sec data. This sliding window was then shifted using a 1 sec step, thus obtaining one coherence measure for each second of data. The Matlab “cohere.m” function was used to calculate auto- and cross-spectrum within each 8 sec data segment with parameters giving a final frequency resolution of 1 Hz: nfft parameter, 512; window size, 1 sec (500 samples); and step, 0.5 sec. Cortical LFP was chosen as the reference and compared with LFP from thalamus, hippocampus, and caudate-putamen. A pooled coherence measure (Amjad et al., 1997; Halliday and Rosenberg, 1999, 2000) was used to combine coherence from individual pairwise comparisons as the overall coherence measure. Briefly, the cross-spectra obtained from all two-channel pairs were summed and normalized for each frequency bin by the sum of the respective auto-spectra from all pairs. The resultant pooled coherence reflects the degree of in-phase oscillations present in all LFPs relative to cortical LFPs and provides a consistent way to look at the coherence structure over multiple LFPs simultaneously with a single measure (Halliday and Rosenberg, 1999, 2000).

Results

LFP characteristics throughout the wake-sleep cycle

The extensive inspection of raw intracranial LFP traces (Fig. 1*A*) confirmed that large-amplitude oscillations were present during all behavioral states, being particularly conspicuous around state transitions (Gottesmann, 1996; Steriade et al., 2001). LFP power spectrograms showed similar state-dependent patterns across the four different forebrain areas (Fig. 1*B*). This redundancy suggests that these areas are synchronously modulated and all informative about the ongoing behavioral state. Different states shared common spectral features, therefore creating ambiguity in a spectrogram-only sorting of behavioral states [e.g., increased theta oscillations (5–9 Hz) during both AE and REM (Fig. 1*B*, white asterisk)]. State transitions occurred simultaneously across all areas.

Global brain states as dynamic spectral trajectories

The 2-D state space revealed a finite number of clusters (Figs. 1*C*, 2*A*) that corresponded to the different behavioral states exhibited by freely behaving rats (Fig. 2*B*). This plot allowed for the unequivocal

identification of most behavioral states (QW, SWS, REM, and WT), as well as the more elusive transient state named IS (Gottesmann, 1973, 1996), or transition state between SWS and REM episodes (Benington et al., 1994; Mandile et al., 1996; Piscopo et al., 2001) (Fig. 2*B*). When LFP spectral amplitude within specific bandwidths was plotted on this state space, it was also possible to further characterize the internal dynamics of individual states. For instance, plotting delta (1–4 Hz) amplitude over the 2-D state space (Fig. 2*C*) broadly separated light SWS (during which 10–14 Hz spindles are predominant) from deep SWS (mostly composed of delta waves). Light and deep SWS constituted a continuous spectrum within the same state, in contrast to the well separated clusters reflecting categorically different global brain states, such as SWS and REM. Moreover, the 2-D state space also provided temporal dynamics information about state evolution, visualized as continuous spectral trajectories as animals coursed from one state to another (Fig. 2*D*). Brief state changes, such as microarousals during SWS episodes (Schieber et al., 1971; Halasz, 1998), could thus be captured (see supplemental Fig. S2, available at www.jneurosci.org as supplemental material). Trajectories connecting different clusters, or state transitions, followed stereotypical spatial paths with characteristic duration. Three of the most frequent trajectories, QW→AE→QW, QW→WT→QW, and QW→SWS→IS→REM→QW, are illustrated in Figure 2*D*. The QW→SWS→QW and QW→SWS→IS→QW sequences were also observed (data not shown). These five cyclic trajectories accounted for the overwhelming majority of the behaviors exhibited by rats across the wake–sleep cycle.

Although a considerable degree of inter-animal variability is to be expected when recording from outbred laboratory animals, we found remarkable similarity across the state spaces obtained for different animals. In five rats, the relative positions of all major and minor states were highly conserved, as can be seen in scatter and density plots (Fig. 3*A,B*, respectively). For instance, the SWS cluster was always located on the upper right quadrant of the state space, whereas IS and REM occupied the left quadrants, and the waking cluster (including AE and QW) occupied the lower right quadrant. When the speed of the spectral trajectories (value obtained by dividing the distance between two consecutive dots in the 2-D space by the time that separates them, i.e., 1 sec) was plotted over the state space (Fig. 3*C*), regions of the state space in which spectral features changed slowly (dark blue) coincided with the three main clusters (Fig. 3, compare *A, B* with *C*), whereas regions of fast spectral change (green–yellow–red) corresponded to transitional zones between major clusters.

Together, these results indicate that the three main clusters, corresponding to waking, SWS, and REM states, represent stable states of forebrain neural activities. On the other hand, transitional zones between clusters with high spectral change speed, including IS, represent periods in which animals shift from one

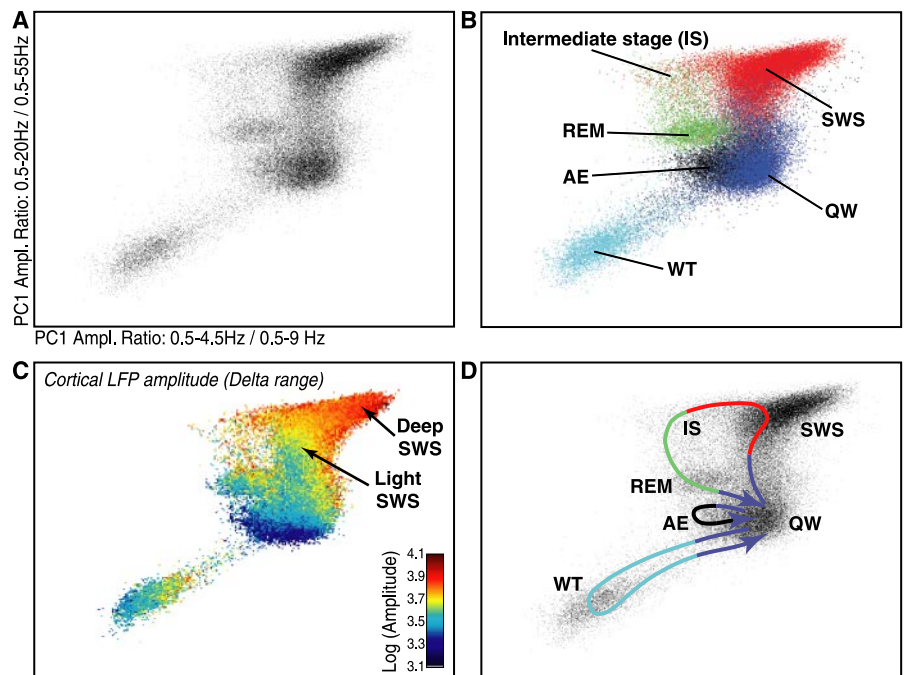


Figure 2. Global brain states and two-dimensional state space. *A*, Scatter plot of the two chosen LFP spectral amplitude ratios, in which four distinct clusters are clearly visible. Each dot corresponds to a 1 sec window for which the amplitude ratios were calculated (48 hr recording, rat 1; for clarity, only one-third of data points, evenly sampled, were plotted). *B*, When color coded according to the behavioral states visually identified, each cluster in the plot corresponds to a distinct state. *C*, The amplitude of cortical LFPs in the delta frequency range (1–4 Hz) is color coded. A fine distinction can be made between light SWS (high spindle density) and deep SWS (mostly composed of delta waves). *D*, Transitions between states can be defined as specific trajectories connecting different clusters, with characteristic duration and speed. Typical trajectories are illustrated. Transitions from SWS to REM always course through the IS region. Trajectories also define the polarity of the different clusters. Entrance to and exit from the SWS cluster always occur on one end of the elongated SWS cluster.

state to another. These results imply that the anatomical and physiological mechanisms governing spectral trajectories across states are conserved among different animals. The sole possible exception is WT, whose cluster occupies a variable location in different rats. Although the overall power spectrum of the WT state was very similar across different rats, with a dominant peak frequency at 7–12 Hz, individual variations were observed in the distribution of resonant (harmonic) frequency peaks (see supplemental Fig. S3, available at www.jneurosci.org as supplemental material), amounting to the inter-animal topographic variation of WT clusters.

Next, we investigated how the information about global brain states is distributed among various forebrain areas by generating state-space maps from the LFPs of each single area in a particular animal (Fig. 4) (see supplemental Fig. S4, available at www.jneurosci.org as supplemental material). The resulting area-specific state-space maps were plotted for each animal and color coded for behavioral states. As predicted from the high redundancy of LFP power spectrograms (Fig. 1*B*), single-area maps were qualitatively similar to the multiple-area pooled maps, except for the cortex-specific maps, in which REM was not well dissociable from other state clusters because of the low contrast (ambiguity) in cortical LFPs between REM and waking in the theta frequency range. This impression was confirmed using a linear discriminant analysis to assess how well each map separates various behavioral states based on the visually coded states (Fig. 4). Error rates were low in all comparisons except for cortex-specific maps for the waking (QW+AE) versus REM and SWS versus REM comparisons in rat 1, 2, and 3. For these comparisons

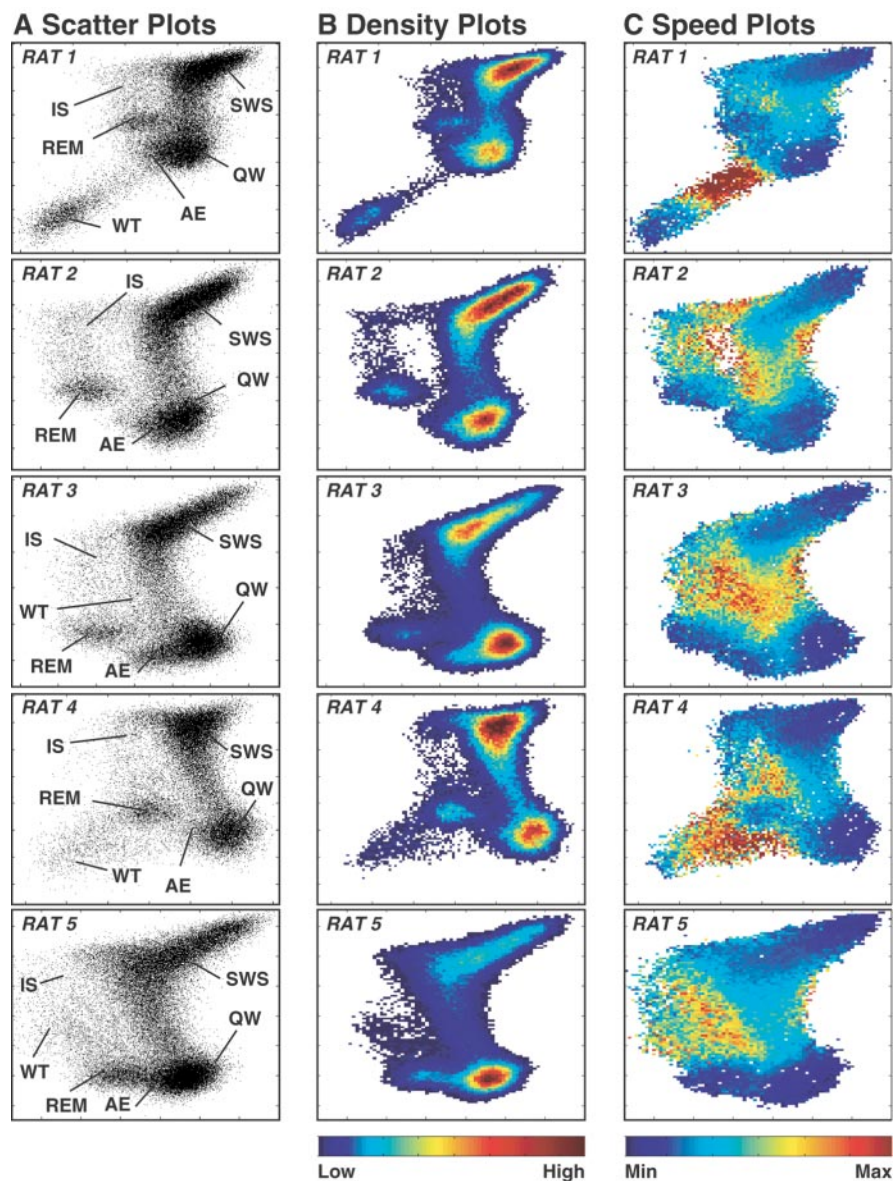


Figure 3. The topography of the two-dimensional state spaces is consistent across animals. *A*, Scatter plots of the 2-D state space (conventions as in Fig. 2*A*). For all animals, 48 hr of recording are displayed; to avoid graphic saturation, only 20% of the data points were evenly sampled and plotted. *B*, Density plots, calculated from the scatter plots, show the conserved cluster topography and the relative abundance of various states (see also Fig. 2*B*). *C*, Speed plots representing the average velocity of spontaneous trajectories within the 2-D state space. Stationarity (low speed) can be observed within the three main clusters, whereas a maximum speed is reached during transitions from one cluster to another (i.e., between brain states).

only, classification errors rates of cortex-derived maps were >1.7-fold those calculated for the overall state-space maps. The all-area state maps, combined using PCA, always successfully captured most of the state information and segregated the clusters close to the best separation offered by individual-area maps. Thus, all-area maps were used as an overall measure for the subsequent state analyses.

The remarkable segregation of clusters in the 2-D state space and its consistency across animals argues that the various behavioral states represent distinct regimens of global forebrain dynamics that can be solely defined by neural signals, thus allowing the development of automatic algorithms capable of accurate classification of global states without reference to behavioral or electromyogram data (Robert et al., 1999; Kohlmorgen et al., 2000; Grube et al., 2002) (see supplemental information and

supplemental Fig. S5, available at www.jneurosci.org as supplemental material).

Functional coupling within the forebrain ensemble across global brain states

To gain additional insight into the dynamics of global brain states, we calculated the coherence between pairs of brain areas and the pooled coherence (Amjad et al., 1997; Halliday and Rosenberg, 1999, 2000) across all recording sites (Figs. 5, 6), which assesses the simultaneous functional coupling among different forebrain areas. When plotted against time, the LFP coherence spectra showed very pronounced state-dependent fluctuations (Fig. 5*A,B*). These state-dependent coherence patterns, present in all pairwise coherence analyses (Fig. 5*A*) (see supplemental Fig. S6, available at www.jneurosci.org as supplemental material), were well captured by the pooled coherence measure (Fig. 5*B*). Thus, pooled coherence provided a consistent measure to look simultaneously at the coherence structure over multiple LFPs with a single measure. A one-way multivariate ANOVA revealed that the pooled coherence for delta (1–4 Hz), theta (5–9 Hz), spindle (10–14 Hz), beta (15–25 Hz), and gamma (30–55 Hz) ranges was significantly different between states ($p < 0.001$). SWS was the state of maximum coherence in the delta and spindle frequency bands (Fig. 5*B*) (0.33 ± 0.09 and 0.27 ± 0.10 , respectively; mean \pm SEM), characterizing the progressive entrainment of all of the forebrain areas by large-amplitude in-phase slow waves (Steriade et al., 1993; Amzica and Steriade, 1995; Achermann and Borbély, 1998a,b; Destexhe et al., 1999). Present during AE, QW, and REM (Maloney et al., 1997; Gross and Gotman, 1999; Uchida et al., 2001), fast gamma oscillations were associated with an overall low pooled coherence during AE, most likely reflecting the absence of gamma coherence over large distances during this state (Destexhe et al., 1999; Gross and Gotman, 1999). In agreement with EEG (Achermann and Borbély, 1998a) and magneto-encephalographic (Linas and Ribary, 1993) evidence in humans, REM was the state of maximum pooled coherence in the gamma range (0.22 ± 0.08 ; mean \pm SEM), indicating a stronger functional coupling between forebrain areas during this state (Fig. 5*B*, REM episodes from 5640 to 5785 sec and from 6116 to 6328 sec). As illustrated in Figure 5*C*, the state-dependent patterns of pooled coherence were confirmed by plotting the coherence measurements on the 2-D state maps. These plots further revealed distinctions within the major states, such as the graded difference between light and deep SWS, and a marked contrast between AE and QW states within the waking state. Indeed, the highest delta pooled coherence values were observed in the right part of the SWS cluster corresponding to deep SWS.

High spindle coherence values were observed during IS and WT (Fig. 6) and to a lesser extent during light SWS. Interestingly, theta coherence was high throughout REM episodes in all brain area pairs [e.g., Cx–Hi (Fig. 5A,C)] but low when calculated across the ensemble (Fig. 5B), indicating a low degree of in-phase theta activity among the ensemble during this state.

As illustrated in Figure 6, the use of pooled coherence from 7–55 Hz as a third dimension of the state space greatly improves the separation between states and further separates WT from the other states because of its high coherence values. For example, in the case of rats 3 and 5, WT appeared undifferentiated at the 2-D plot (Figs. 3A, 5C) but could be clearly separated from the other states on the 3-D representation (Fig. 6). This reflects the fact that the state with the highest LFP pooled coherence in the forebrain was WT, spanning broad frequency bands (7–12, 14–18, and 20–28 Hz) (Figs. 5B, 7, third column) (see supplemental Fig. S3, available at www.jneurosci.org as supplemental material).

Forebrain dynamics during state transitions

To further scrutinize the neural dynamics underlying transitions between global brain states, we quantified the stereotypical trajectory patterns bridging major states in the 2-D state space. Common state-to-state transitions (Fig. 7, left panels) can be easily identified by a parametric analysis of trajectory paths and their duration (Fig. 7, middle panels) (see supplemental Fig. S7, available at www.jneurosci.org as supplemental material). Whereas most state transitions were direct and fast (QW→SWS at 11.02 ± 0.36 sec; REM→QW at 3.50 ± 0.11 sec; mode \pm SEM), transitions involving IS [e.g., SWS→REM transition (Fig. 7B,B')] lasted considerably longer (26.67 ± 0.36 sec; mode \pm SEM; $F_{(7,40)} = 85.70$; $p < 0.001$; one-way ANOVA, followed by LSD *post hoc* test).

Regardless of differences in duration, almost all state transitions involved striking changes in forebrain LFP synchronization manifested in the coherence spectra (Fig. 7, right panels) (see supplemental Fig. S8, available at www.jneurosci.org as supplemental material). Significant coherence changes during state transitions were identified by comparing the coherence spectra of state transitions with the spectrum of the flanking states. REM→QW transitions showed the least changes of coherence spectrum among all successive states (Fig. 7C'). For the QW→SWS transitions, we observed a significant change of coherence in the spindle frequency range (Fig. 7A'') relative to both QW and SWS ($p = 0.025$ and $p = 0.043$ respectively; paired Student's *t* test). We also found a significant increase in delta range coherence when comparing the QW→SWS transitions with SWS ($p = 0.007$; paired Student's *t* test). Interestingly, delta

Area-specific state-space maps and the separation of states

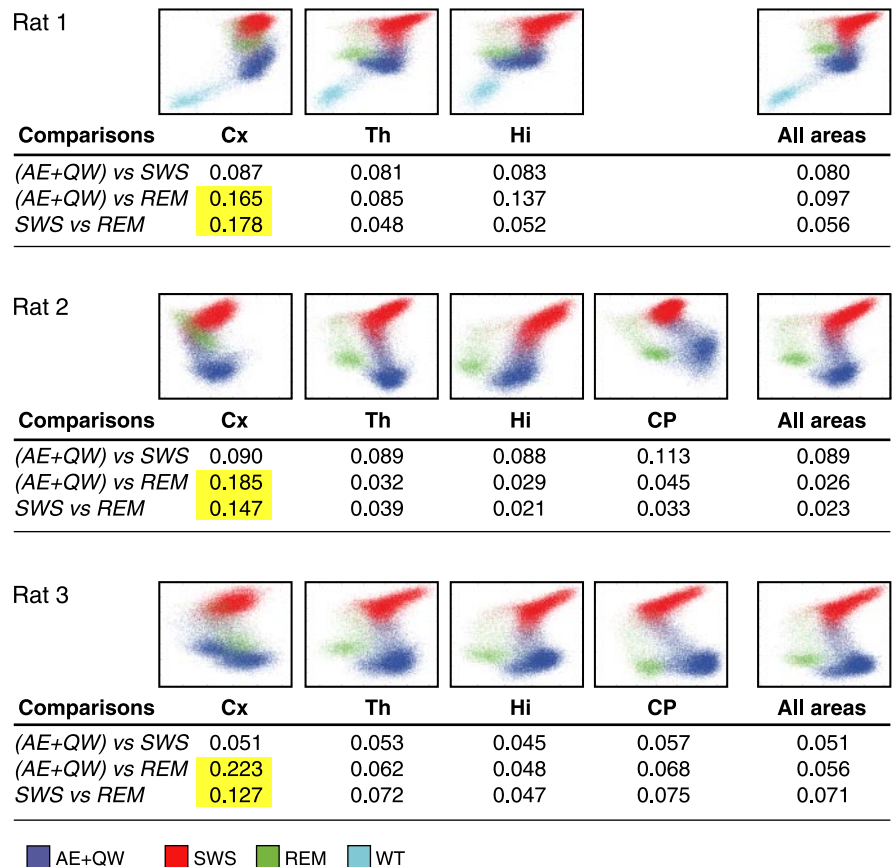
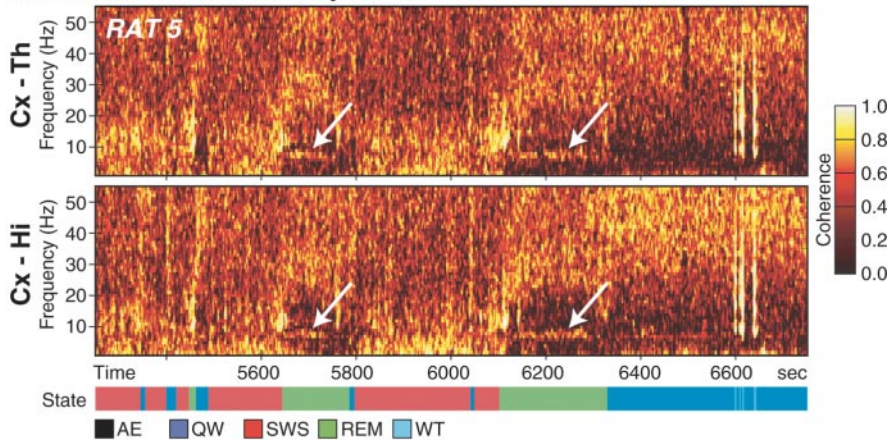


Figure 4. Area-specific state maps. Individual area state maps generated for three rats and color coded for the behavioral state. PCA was used to combine amplitude ratios obtained from different LFPs (rightmost column). Forty-eight hours of data were plotted for each animal (subsampling 1/3 of data for clarity). Rat 1 was not implanted for recording in the CP. Compared with the state space generated by combining LFPs from all areas, all area-specific maps show qualitatively similar separation of major behavioral states, except for cortex-specific maps. This difference was quantified using linear discriminant analysis to assess how well each map separates the various behavioral states based on the visually coded states. The error rates in the tables represent the proportion of misclassification when an optimal linear decision boundary was used to discriminate the two selected states. Only the highlighted combinations (yellow) show > 1.7 -fold classification error compared with the error rate in the overall state-space map. These high error rate combinations came exclusively from cortex-specific maps in the (AE+QW) versus REM and SWS versus REM comparisons. The results indicate that single-area maps provide as much information as multiple-area pooled maps with regard to state classification. There is therefore a certain redundancy among the forebrain areas studied, with the possible exception of cortex.

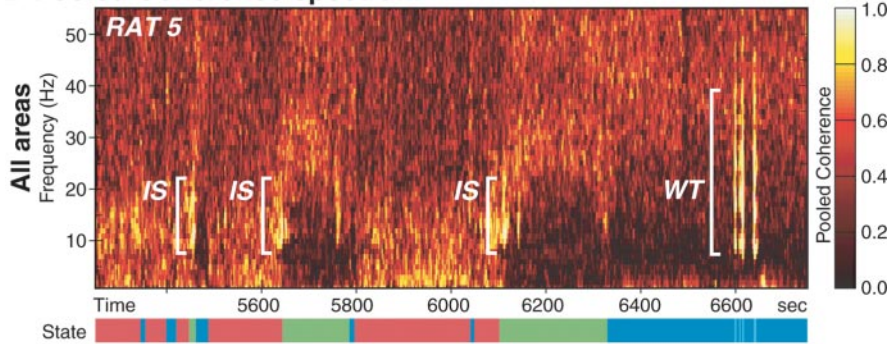
coherence during the transition was very similar to that observed during QW ($p = 0.046$; paired Student's *t* test) and significantly lower than the average of QW and SWS values, ($p = 0.012$; paired Student's *t* test), whereas no significant difference was found at spindle range ($p = 0.201$; paired Student's *t* test). Altogether, these results indicate that delta coherence changes were slower and less prominent than changes in spindle coherence, supporting the notion that transitions into SWS mainly involve changes in the magnitude of spindle coherence (Achermann and Borbely, 1998b).

Dramatic changes in coherence spectra were even more pronounced in transitions involving IS: the pooled coherence amplitude during SWS→IS→REM transitions was significantly higher than the expected average of SWS and REM between 7 and 22 Hz ($p = 0.01$; paired Student's *t* test) and peaked at 8–12 Hz (Fig. 7B'') (see also Fig. 5A,B), which corresponds to the frequency band of the large-amplitude oscillations that characterize IS (Mandile et al., 1996). Similar increases in coherence could

A Pairwise Coherence spectra



B Pooled Coherence spectrum



C Coherence on 2-D maps

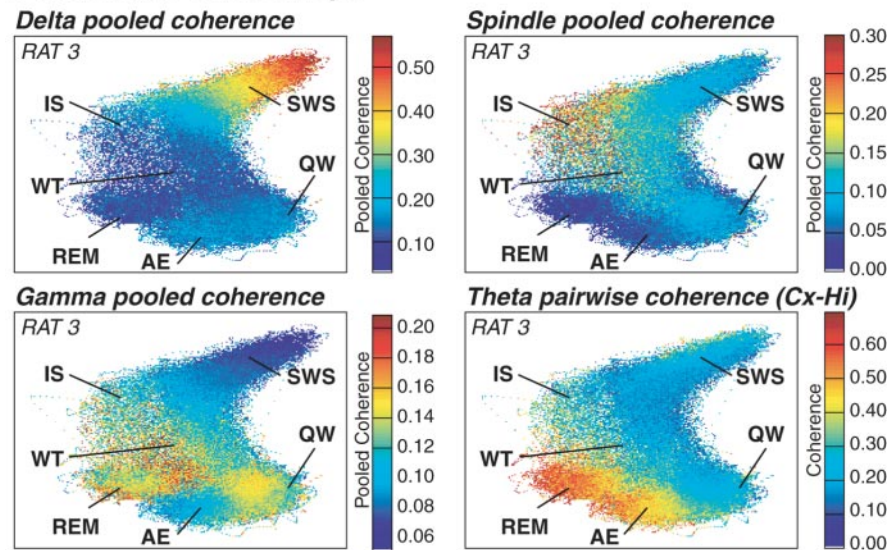


Figure 5. LFP coherence analysis. *A*, Examples of pairwise coherence spectrograms illustrating the state-dependent pattern of coupling between Cx and Th (top) and between Cx and Hi (bottom). The spectrograms are aligned with the behavioral state identification (visual coding). Notice that, during REM sleep, both pairs of areas present a high coherence in the theta frequency range (white arrows). *B*, LFP pooled coherence spectrogram showing the variations of coherence across all areas during the wake–sleep cycle. The highest pooled coherence values are observed in the low frequency range (delta range) during SWS episodes. During WT, animals present typical 7–12 Hz LFP oscillations, and the pooled coherence is greatly increased in this frequency range and its harmonics. The IS state shows high pooled coherence in the 7–22 Hz range. REM and QW have the highest pooled coherence in the gamma range (>30 Hz) but also a low pooled coherence in the theta range, indicating that the four areas present theta oscillations that are not strictly in-phase. *C*, Coherence measurements over 48 hr of recording are overlaid on the 2-D state map. For delta, spindle, and gamma frequency ranges, pooled coherence is shown. In the theta range, pairwise coherence between Cx and Hi is displayed. High delta pooled coherence values are observed in the right portion of the SWS cluster corresponding to deep SWS, whereas high spindle coherence values are observed during IS and WT (see also Fig. 6). High gamma pooled coherence is observed during both REM and QW. The pair Cx–Hi presents high theta coherence during both REM and AE.

also be found in other state transitions involving IS, such as SWS→IS→QW and REM→IS→QW (data not shown). For QW→WT transitions, the resonant peaks of coherence were consistently shifted toward higher frequencies relative to those of the WT state (Fig. 7*D''*), suggesting the presence of transient increased coherence at higher frequencies, at the beginning of WT epochs (Shaw, 2003).

Discussion

In the simple state-space framework described here, based on forebrain LFPs, all major global brain states can be consistently and unambiguously identified as distinct spectral clusters within a global dynamic structure formed by the combined activity of forebrain ensembles recorded from the cortical, thalamic, hippocampal, and striatal networks. Subtle distinctions can be found within the major states, such as the graded difference between light and deep SWS, and the AE and QW states within the waking state.

Whereas AE, QW, WT, SWS, and REM can be considered as categorically distinct stable global brain states, IS appears as a transient state characterized by widespread forebrain synchronization. Our results offer strong independent evidence that IS constitutes a distinct transitional state, resembling neither SWS nor REM (Gottesmann, 1996; Mandile et al., 1996). State transitions occur through specific trajectories within the global dynamic structure revealed by the state space, each of them with a characteristic duration, spectral path, and coherence bandwidth. Transitions between most global brain states involve striking changes of LFP coherence across forebrain areas, supporting the idea that all major behavioral states represent different dynamic regimens of neural processing.

Physiological significance of the 3-D state space

Our results are in line with numerous studies showing that behavioral state-related rhythms recorded by surface EEG are also present in subcortical areas. For instance, beta oscillations recorded in the motor cortex during voluntary movements (Sanes and Donoghue, 1993) have also been recorded in the hippocampus (Leung, 1992) and more recently in the striatum (Courtemanche et al., 1997, 2003). Fast gamma oscillations (30–80 Hz) associated with activation of cortical sensory areas (Buzsaki et al., 1992; Singer and Gray, 1995) have also been reported in the hippocampus of rodents and humans

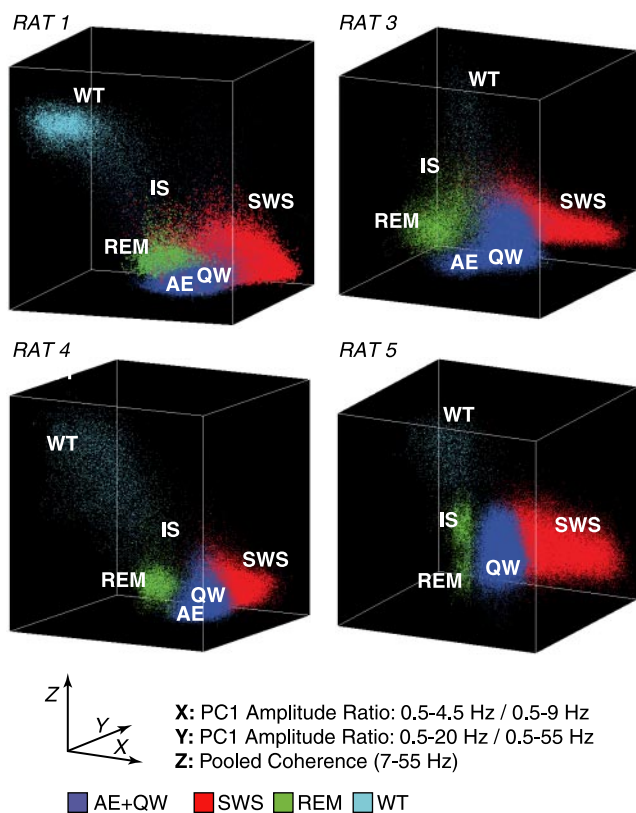


Figure 6. Pooled coherence, a single measure to address the dynamic of global brain states. 3-D state space in four rats derived from the two amplitude ratios (*X*- and *Y*-axes) and the additional average pooled coherence between 7 and 55 Hz (*Z*-axis). The use of pooled coherence as a single measure of the coupling between forebrain areas captured state-dependent patterns and further improved the separation between states. Notice that the WT cluster can be easily identified.

(Borbely et al., 1984; Buzsaki et al., 1992). Here we show that LFPs from the cortex, thalamus, hippocampus, and striatum evolve similarly and simultaneously across all states that comprise the wake–sleep cycle.

It is well known that LFPs mostly reflect synaptic currents, i.e., the summation of postsynaptic potentials and intrinsic currents (Nunez, 1981; Lopes da Silva, 1991). It is also known that the amplitude of LFP signals is correlated to the degree of coherent activity in a population of neurons (Lopes da Silva, 1991). In a freely behaving animal, synaptic currents generated by local networks and short-range connections are not easily dissociable from those caused by distant synaptic projections (Cauller and Connors, 1994; Castro-Alamancos and Connors, 1996). The changes in LFP signals observed concurrently within four forebrain structures captured by the 3-D state space reflect the global synaptic input landscape underlying the activity of forebrain neurons. These changes probably do not derive from a single common source but rather from the local integration of local, regional, and global inputs. This point is particularly well illustrated by the low pooled coherence in the theta band during AE and REM, states characterized by strong hippocampal theta rhythm (Green and Arduini, 1954; Timo-Iaria et al., 1970).

The 3-D dynamic landscape is primarily determined by ascending neuromodulatory systems, including the pontine and basal forebrain cholinergic nuclei, and the monoaminergic systems in the brainstem (Jouvet, 1962, 1972; Moruzzi, 1972; Jones, 1991, 1993; Steriade et al., 1993; Berridge and Waterhouse, 2003). These interconnected systems (Nauta et al., 1974; Nauta, 1979;

Steriade and Deschenes, 1984; Jones, 1993; Zaborszky et al., 1999; Killackey and Sherman, 2003) lead to the state-dependent delivery of modulatory neurotransmitters throughout the entire forebrain, shaping the synaptic landscape that gates neuronal responses and behavior. As a result, the activity of neuronal populations in multiple forebrain areas evolves simultaneously across the wake–sleep cycle according to complex and dynamic state-specific patterns (Winson and Abzug, 1977; Pavlides et al., 1988; Steriade et al., 2001; Berridge and Waterhouse, 2003). In support of this view, studies in awake monkeys performing a visual search task have shown that responses to visual stimulation recorded in cortical area V4 were often reduced or even completely blocked when animals became drowsy, whereas the background neuronal activity changed to the burst-pause pattern typically observed in sleep (Pigarev et al., 1997). Similarly, state-dependent alterations of auditory receptive fields have been reported in rats (Edeline et al., 2000). In the somatosensory system of rats, it has been shown recently that behavioral change during waking states (QW, AE, and WT) determines parallel changes in the tactile responses of neuronal ensembles in the main thalamo-cortical loop of the trigeminal system (Fanselow and Nicolelis, 1999; Nicolelis and Fanselow, 2002; Wiest and Nicolelis, 2003). Enhancements of neuronal responsiveness by changes in synaptic background activity have also been reported in computational studies (Ho and Destexhe, 2000). In conclusion, the accurate identification of global brain state within a synaptic input landscape such as the one presented in this study is likely to provide substantial insight about the effects of central states on evoked responses and spontaneous behaviors.

Functional coupling of brain areas during state transitions

The interest in measures of neural coherence to study global brain states derives from the fact that waking and sleep involve very different levels of in-phase LFP oscillations. The fast LFP oscillations that characterize waking occur simultaneously in multiple cortical spots but result in overall low coherence over long distances (Destexhe et al., 1999). In contrast, SWS is characterized by a gradual increase of low-frequency LFP coherence (Steriade et al., 1993; Achermann and Borbely, 1998a,b; Destexhe et al., 1999). Here, we presented for the first time direct evidence that global brain state transitions occur simultaneously across multiple forebrain areas as transient and drastic changes in neural synchronization. These changes are effected by the prominent narrow-band neural oscillations that mark state boundaries. Our results show that distant forebrain areas tightly coordinate the processing of neural information as one global brain state evolves into another, indicating a very high degree of functional integration in the forebrain across the entire wake–sleep cycle.

Our results also clearly indicate that the extent of functional coupling across multiple forebrain areas in the theta and gamma ranges is smaller than in the delta frequency band, supporting the inverse relationship between synchronization–frequency and the distance between functionally connected areas, i.e., long-range synchronization at low frequencies and short-distance coupling at high frequencies (Achermann and Borbely, 1998a; Gross and Gotman, 1999; von Stein and Sarnthein, 2000).

Synchronization within neuronal ensembles and coherence among interconnected brain areas have been proposed to underlie the integration of behavior (Hebb, 1949; Nicolelis et al., 1995; Singer, 1995; Engel et al., 2001; Varela et al., 2001; O'Connor et al., 2002). Our data indicate that the spontaneous succession of global brain states is nearly always accompanied by marked changes in LFP coherence at selected frequency bands across

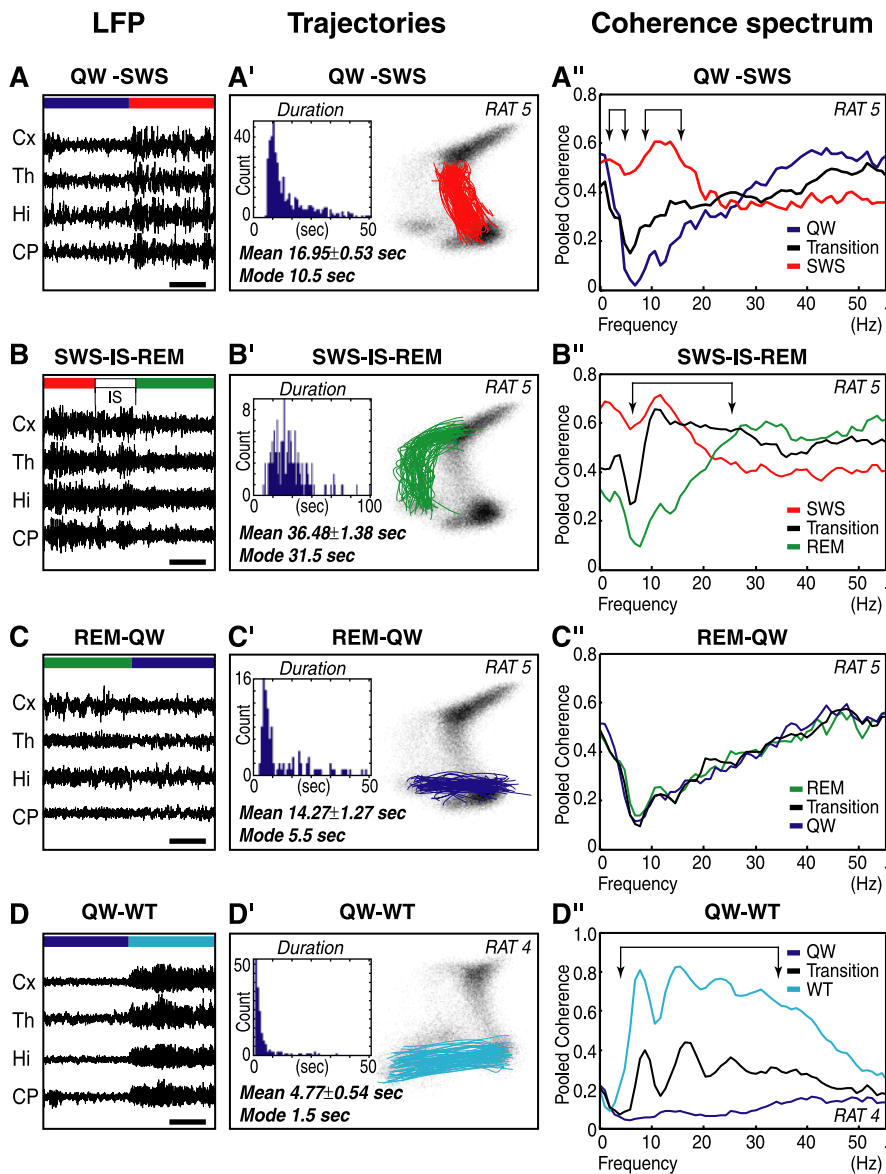


Figure 7. Coherence spectra at state transitions. Four common global brain state transitions of a representative animal are presented with an example of LFP recordings (first column), the corresponding spectral trajectories and their duration within the 2-D state space (second column), and an averaged pooled coherence spectrum for the pre- and post-states and the transition itself (third column). LFP, Recordings of the four areas revealed common oscillatory features and simultaneous changes during state transitions. Calibration bar, 5 sec. Trajectories, Paths connecting major clusters were identified, and histograms of the distribution of duration (insets) were calculated for these trajectories. The average and mode \pm SEM of the duration are indicated for this animal (see supplemental Fig. S7, available at www.jneurosci.org as supplemental material). Coherence spectrum, Average coherence spectrum of transitions plotted against the average coherence spectrum of the pre- and post-states, whose points were taken from time points immediately adjacent to the selected trajectories with the same duration as the trajectory. Arrows indicate frequency bands at which significant changes in LFP coherence occur during the transition.

multiple forebrain areas. Transitions between states with very different coherence bandwidths thus seem to require either gradual spectral change at selected bandwidths, or abrupt broadband synchronization. These distributed and highly coherent LFP oscillations presumably reflect transient synchronizations of synaptic inputs at the termination and initiation of global brain states. We propose that such transient synchronization at the boundaries of global states may function as a “handshake protocol” within and across brain areas. By simultaneously adjusting the functional connectivity between areas (Glenn and Steriade, 1982; Lopes da Silva, 1991), these transient events may allow spatially distributed structures to orga-

nize and share a continuous flow of information throughout the wake–sleep cycle, building neural representations in a state-dependent manner.

From a behavioral point of view, a mechanism to facilitate the exchange of neural information within and across brain areas may be critical when animals shift from waking to sleep. Whereas wakefulness can be described as a state for real-time processing of sensorimotor information, sleep is rather involved in the off-line processing and consolidation of newly acquired information (Jenkins and Dallenbach, 1924; Fishbein, 1971; Hennevin et al., 1971; Smith et al., 1980; Smith and Butler, 1982; Buzsaki, 1989; Pavlides and Winson, 1989; Wilson and McNaughton, 1994; Hennevin et al., 1995; Stickgold, 1998; Laureys et al., 2001; Maquet, 2001; Stickgold et al., 2001; Ribeiro et al., 2004). A stronger functional coupling between areas at the boundaries of waking and sleep states might not only ensure a sustained and accurate transfer of sensorimotor information but also allow an overall reinforcement of selected pathways, further promoting the consolidation of specific memory traces acquired during waking.

References

- Achermann P, Borbely AA (1997) Low-frequency (<1 Hz) oscillations in the human sleep electroencephalogram. *Neuroscience* 81:213–222.
- Achermann P, Borbely AA (1998a) Coherence analysis of the human sleep electroencephalogram. *Neuroscience* 85:1195–1208.
- Achermann P, Borbely AA (1998b) Temporal evolution of coherence and power in the human sleep electroencephalogram. *J Sleep Res* 7 [Suppl 1]:36–41.
- Amjad AM, Halliday DM, Rosenberg JR, Conway BA (1997) An extended difference of coherence test for comparing and combining several independent coherence estimates: theory and application to the study of motor units and physiological tremor. *J Neurosci Methods* 73:69–79.
- Amzica F, Steriade M (1995) Short- and long-range neuronal synchronization of the slow (<1 Hz) cortical oscillation. *J Neurophysiol* 73:20–38.
- Benington JH, Kodali SK, Heller HC (1994) Scoring transitions to REM sleep in rats based on the EEG phenomena of pre-REM sleep: an improved analysis of sleep structure. *Sleep* 17:28–36.
- Berger H (1929) Über das Elektroencephalogramm des menschen. *Arch Psychiatr* 87:527–570.
- Berridge CW, Waterhouse BD (2003) The locus coeruleus-noradrenergic system: modulation of behavioral state and state-dependent cognitive processes. *Brain Res Brain Res Rev* 42:33–84.
- Bland BH (1986) The physiology and pharmacology of hippocampal formation theta rhythms. *Prog Neurobiol* 26:1–54.
- Blazquez PM, Fujii N, Kojima J, Graybiel AM (2002) A network representation of response probability in the striatum. *Neuron* 33:973–982.

- Borbely AA, Tobler I, Hanagasioglu M (1984) Effect of sleep deprivation on sleep and EEG power spectra in the rat. *Behav Brain Res* 14:171–182.
- Brown LL, Schneider JS, Lidsky TI (1997) Sensory and cognitive functions of the basal ganglia. *Curr Opin Neurobiol* 7:157–163.
- Buzsaki G (1989) Two-stage model of memory trace formation: a role for “noisy” brain states. *Neuroscience* 31:551–570.
- Buzsaki G, Chen LS, Gage FH (1990) Spatial organization of physiological activity in the hippocampal region: relevance to memory formation. *Prog Brain Res* 83:257–268.
- Buzsaki G, Horvath Z, Urioste R, Hetke J, Wise K (1992) High-frequency network oscillation in the hippocampus. *Science* 256:1025–1027.
- Castro-Alamancos MA, Connors BW (1996) Spatiotemporal properties of short-term plasticity sensorimotor thalamocortical pathways of the rat. *J Neurosci* 16:2767–2779.
- Caton R (1875) The electric currents of the brain. *Br Med J* 2:278.
- Cauler LJ, Connors BW (1994) Synaptic physiology of horizontal afferents to layer I in slices of rat SI neocortex. *J Neurosci* 14:751–762.
- Courtemanche R, Sun GD, Lamarre Y (1997) Movement-related modulation across the receptive field of neurons in the primary somatosensory cortex of the monkey. *Brain Res* 777:170–178.
- Courtemanche R, Fujii N, Graybiel AM (2003) Synchronous, focally modulated β -band oscillations characterize local field potential activity in the striatum of awake behaving monkeys. *J Neurosci* 23:11741–11752.
- Dement WC, Kleitman N (1957) Cyclic variations in EEG during sleep and their relation to eye movements, body motility and dreaming. *Electroencephalogr Clin Neurophysiol* 20:673–690.
- Destexhe A, Contreras D, Steriade M (1999) Spatiotemporal analysis of local field potentials and unit discharges in cat cerebral cortex during natural wake and sleep states. *J Neurosci* 19:4595–4608.
- Edeline JM, Manunta Y, Hennevin E (2000) Auditory thalamus neurons during sleep: changes in frequency selectivity, threshold, and receptive field size. *J Neurophysiol* 84:934–952.
- Engel AK, Fries P, Singer W (2001) Dynamic predictions: oscillations and synchrony in top-down processing. *Nat Rev Neurosci* 2:704–716.
- Fanselow EE, Nicolelis MA (1999) Behavioral modulation of tactile responses in the rat somatosensory system. *J Neurosci* 19:7603–7616.
- Fishbein W (1971) Disruptive effects of rapid eye movement sleep deprivation on long-term memory. *Physiol Behav* 6:279–282.
- Gastaut H (1952) Electroencephalographic study of the reactivity of rolandic rhythms (in French). *Rev Neurol* 87:176–182.
- Glenn LL, Steriade M (1982) Discharge rate and excitability of cortically projecting intralaminar thalamic neurons during waking and sleep states. *J Neurosci* 2:1387–1404.
- Gottesmann C (1973) Intermediate stages of sleep in the rat (in French). *Rev Electroencephalogr Neurophysiol Clin* 3:65–68.
- Gottesmann C (1996) The transition from slow-wave sleep to paradoxical sleep: evolving facts and concepts of the neurophysiological processes underlying the intermediate stage of sleep. *Neurosci Biobehav Rev* 20:367–387.
- Graybiel AM (1997) The basal ganglia and cognitive pattern generators. *Schizophr Bull* 23:459–469.
- Green JD, Arduini AA (1954) Hippocampal electrical activity in arousal. *J Neurophysiol* 17:533–557.
- Gross DW, Gotman J (1999) Correlation of high-frequency oscillations with the sleep-wake cycle and cognitive activity in humans. *Neuroscience* 94:1005–1018.
- Grube G, Flexer A, Dorffner G (2002) Unsupervised continuous sleep analysis. *Methods Find Exp Clin Pharmacol* 24 [Suppl D]:51–56.
- Halasz P (1998) Hierarchy of micro-arousals and the microstructure of sleep. *Neurophysiol Clin* 28:461–475.
- Halliday DM, Rosenberg JR (1999) Time and frequency domain analysis of spike train and time series data. In: *Modern techniques in neuroscience research* (Windhorst U, Johansson H, eds), pp 503–543. Berlin: Springer.
- Halliday DM, Rosenberg JR (2000) On the application, estimation and interpretation of coherence and pooled coherence. *J Neurosci Methods* 100:173–174.
- Hari R, Salmelin R (1997) Human cortical oscillations: a neuromagnetic view through the skull. *Trends Neurosci* 20:44–49.
- Hebb DO (1949) *The organization of behavior: a neuropsychological theory*. New York: Wiley.
- Hennevin E, Leconte P, Bloch V (1971) Effect of acquisition level on the increase of paradoxical sleep duration due to an avoidance conditioning in the rat (in French). *C R Acad Sci Hebd Seances Acad Sci D* 273:2595–2598.
- Hennevin E, Hars B, Maho C, Bloch V (1995) Processing of learned information in paradoxical sleep: relevance for memory. *Behav Brain Res* 69:125–135.
- Ho N, Destexhe A (2000) Synaptic background activity enhances the responsiveness of neocortical pyramidal neurons. *J Neurophysiol* 84:1488–1496.
- Hobson JA, Pace-Schott EF (2002) The cognitive neuroscience of sleep: neuronal systems, consciousness and learning. *Nat Rev Neurosci* 3:679–693.
- Jenkins JG, Dallenbach KM (1924) Oblivescence during sleep and waking. *Am J Psychol* 35:605–612.
- Jones BE (1991) The role of noradrenergic locus coeruleus neurons and neighboring cholinergic neurons of the pontomesencephalic tegmentum in sleep-wake states. *Prog Brain Res* 88:533–543.
- Jones BE (1993) The organization of central cholinergic systems and their functional importance in sleep-waking states. *Prog Brain Res* 98:61–71.
- Jouvet M (1962) Recherche sur les structures nerveuses et les mécanismes responsables des différentes phases du sommeil physiologique. *Arch Ital Biol* 100:125–206.
- Jouvet M (1972) The role of monoamines and acetylcholine-containing neurons in the regulation of the sleep-waking cycle. *Ergeb Physiol* 64:166–307.
- Killackey HP, Sherman SM (2003) Corticothalamic projections from the rat primary somatosensory cortex. *J Neurosci* 23:7381–7384.
- Kohlmorgen J, Muller KR, Rittweger J, Pawelzik K (2000) Identification of nonstationary dynamics in physiological recordings. *Biol Cybern* 83:73–84.
- Laureys S, Peigneux P, Phillips C, Fuchs S, Degueldre C, Aerts J, Del Fiore G, Petiau C, Luxen A, van der Linden M, Cleeremans A, Smith C, Maquet P (2001) Experience-dependent changes in cerebral functional connectivity during human rapid eye movement sleep. *Neuroscience* 105:521–525.
- Leung LS (1992) Fast (beta) rhythms in the hippocampus: a review. *Hippocampus* 2:93–98.
- Llinas R, Ribary U (1993) Coherent 40-Hz oscillation characterizes dream state in humans. *Proc Natl Acad Sci USA* 90:2078–2081.
- Lopes da Silva F (1991) Neural mechanisms underlying brain waves: from neural membranes to networks. *Electroencephalogr Clin Neurophysiol* 79:81–93.
- Maloney KJ, Cape EG, Gotman J, Jones BE (1997) High-frequency gamma electroencephalogram activity in association with sleep-wake states and spontaneous behaviors in the rat. *Neuroscience* 76:541–555.
- Mandile P, Vescia S, Montagnese P, Romano F, Onio Giuditta A (1996) Characterization of transition sleep episodes in baseline EEG recordings of adult rats. *Physiol Behav* 60:1435–1439.
- Maquet P (1997) Positron emission tomography studies of sleep and sleep disorders. *J Neurol* 244:S23–S28.
- Maquet P (1999) Brain mechanisms of sleep: contribution of neuroimaging techniques. *J Psychopharmacol* 13:S25–S28.
- Maquet P (2001) The role of sleep in learning and memory. *Science* 294:1048–1052.
- McCormick DA (2002) Cortical and subcortical generators of normal and abnormal rhythmicity. *Int Rev Neurobiol* 49:99–114.
- McCormick DA, Bal T (1997) Sleep and arousal: thalamocortical mechanisms. *Annu Rev Neurosci* 20:185–215.
- McNaughton BL, Barnes CA, Rao G, Baldwin J, Rasmussen M (1986) Long-term enhancement of hippocampal synaptic transmission and the acquisition of spatial information. *J Neurosci* 6:563–571.
- Moruzzi G (1972) The sleep-waking cycle. *Ergeb Physiol* 64:1–165.
- Nauta HJ (1979) A proposed conceptual reorganization of the basal ganglia and telencephalon. *Neuroscience* 4:1875–1881.
- Nauta HJ, Pritz MB, Lasek RJ (1974) Afferents to the rat caudoputamen studied with horseradish peroxidase. An evaluation of a retrograde neuroanatomical research method. *Brain Res* 67:219–238.
- Nicolelis MA, Fanselow EE (2002) Thalamocortical optimization of tactile processing according to behavioral state. *Nat Neurosci* 5:517–523.
- Nicolelis MA, Baccala LA, Lin RC, Chapin JK (1995) Sensorimotor encoding by synchronous neural ensemble activity at multiple levels of the somatosensory system. *Science* 268:1353–1358.
- Nicolelis MA, Ghazanfar AA, Faggin BM, Votaw S, Oliveira LM (1997) Re-

- constructing the engram: simultaneous, multisite, many single neuron recordings. *Neuron* 18:529–537.
- Nicolelis MA, Dimitrov D, Carmena JM, Crist R, Lehev G, Kralik JD, Wise SP (2003) Chronic, multisite, multielectrode recordings in macaque monkeys. *Proc Natl Acad Sci USA* 100:11041–11046.
- Nunez PL (1981) *Electric fields of the brain: the neurophysics of EEG*, Ed 1. New York: Oxford UP.
- Nunez PL (2000) Toward a quantitative description of large-scale neocortical dynamic function and EEG. *Behav Brain Sci* 23:371–398, 399–437.
- O'Connor SM, Berg RW, Kleinfeld D (2002) Coherent electrical activity between vibrissa sensory areas of cerebellum and neocortex is enhanced during free whisking. *J Neurophysiol* 87:2137–2148.
- Pavlidis C, Winson J (1989) Influences of hippocampal place cell firing in the awake state on the activity of these cells during subsequent sleep episodes. *J Neurosci* 9:2907–2918.
- Pavlidis C, Greenstein YJ, Grudman M, Winson J (1988) Long-term potentiation in the dentate gyrus is induced preferentially on the positive phase of theta-rhythm. *Brain Res* 439:383–387.
- Paxinos G, Watson C (1998) *The rat brain in stereotaxic coordinates*, Ed 4. San Diego: Academic.
- Pigarev IN, Nothdurft HC, Kastner S (1997) Evidence for asynchronous development of sleep in cortical areas. *NeuroReport* 8:2557–2560.
- Piscopo S, Mandile P, Montagnese P, Cotugno M, Giuditta A, Vescia S (2001) Identification of trains of sleep sequences in adult rats. *Behav Brain Res* 119:93–101.
- Ribeiro S, Gervasoni D, Soares ES, Zhou Y, Lin SC, Pantoja J, Lavine M, Nicolelis MAL (2004) Long-lasting novelty-induced neuronal reverberation during slow-wave sleep in multiple forebrain areas. *PLoS Biol* 2:126–137.
- Robert C, Guilpin C, Limoge A (1999) Automated sleep staging systems in rats. *J Neurosci Methods* 88:111–122.
- Sanes JN, Donoghue JP (1993) Oscillations in local field potentials of the primate motor cortex during voluntary movement. *Proc Natl Acad Sci USA* 90:4470–4474.
- Schieber JP, Muzet A, Ferriere PJ (1971) Phases of spontaneous transitory activation during normal sleep in humans (in French). *Arch Sci Physiol (Paris)* 25:443–465.
- Shaw FZ (2003) Is spontaneous high-voltage rhythmic spike discharge in Long Evans rats an absence-like seizure activity? *J Neurophysiol* 91:63–77.
- Singer W (1995) Development and plasticity of cortical processing architectures. *Science* 270:758–764.
- Singer W, Gray CM (1995) Visual feature integration and the temporal correlation hypothesis. *Annu Rev Neurosci* 18:555–586.
- Smith C, Butler S (1982) Paradoxical sleep at selective times following training is necessary for learning. *Physiol Behav* 29:469–473.
- Smith C, Young J, Young W (1980) Prolonged increases in paradoxical sleep during and after avoidance-task acquisition. *Sleep* 3:67–81.
- Squire LR (1986) Mechanisms of memory. *Science* 232:1612–1619.
- Steriade M (1993) Central core modulation of spontaneous oscillations and sensory transmission in thalamocortical systems. *Curr Opin Neurobiol* 3:619–625.
- Steriade M (2003) The corticothalamic system in sleep. *Front Biosci* 8:d878–d899.
- Steriade M, Deschenes M (1984) The thalamus as a neuronal oscillator. *Brain Res* 320:1–63.
- Steriade M, McCormick DA, Sejnowski TJ (1993) Thalamocortical oscillations in the sleeping and aroused brain. *Science* 262:679–685.
- Steriade M, Timofeev I, Grenier F (2001) Natural waking and sleep states: a view from inside neocortical neurons. *J Neurophysiol* 85:1969–1985.
- Stickgold R (1998) Sleep: off-line memory reprocessing. *Trends Cogn Sci* 2:484–492.
- Stickgold R, Hobson JA, Fosse R, Fosse M (2001) Sleep, learning, and dreams: off-line memory reprocessing. *Science* 294:1052–1057.
- Timo-Iaria C, Negro N, Schmidek WR, Hoshino K, Lobato de Menezes CE, Leme da Rocha T (1970) Phases and states of sleep in the rat. *Physiol Behav* 5:1057–1062.
- Uchida S, Maehara T, Hirai N, Okubo Y, Shimizu H (2001) Cortical oscillations in human medial temporal lobe during wakefulness and all-night sleep. *Brain Res* 891:7–19.
- Vanderwolf CH (1969) Hippocampal electrical activity and voluntary movement in the rat. *Electroencephalogr Clin Neurophysiol* 26:407–418.
- Varela F, Lachaux JP, Rodriguez E, Martinerie J (2001) The brainweb: phase synchronization and large-scale integration. *Nat Rev Neurosci* 2:229–239.
- von Stein A, Sarnthein J (2000) Different frequencies for different scales of cortical integration: from local gamma to long range alpha/theta synchronization. *Int J Psychophysiol* 38:301–313.
- Werth E, Achermann P, Dijk DJ, Borbely AA (1997) Spindle frequency activity in the sleep EEG: individual differences and topographic distribution. *Electroencephalogr Clin Neurophysiol* 103:535–542.
- Wiest MC, Nicolelis MA (2003) Behavioral detection of tactile stimuli during 7–12 Hz cortical oscillations in awake rats. *Nat Neurosci* 6:913–914.
- Wilson MA, McNaughton BL (1994) Reactivation of hippocampal ensemble memories during sleep. *Science* 265:676–679.
- Winson J (1974) Patterns of hippocampal theta rhythm in the freely moving rat. *Electroencephalogr Clin Neurophysiol* 36:291–301.
- Winson J, Abzug C (1977) Gating of neuronal transmission in the hippocampus: efficacy of transmission varies with behavioral state. *Science* 196:1223–1225.
- Zaborszky L, Pang K, Somogyi J, Nadasdy Z, Kallo I (1999) The basal forebrain corticopetal system revisited. *Ann NY Acad Sci* 877:339–367.